



Introductory Lectures: Applying Perturbation and Related Methods to Rationally Describe the “Teapot Effect” Under Capillary and Weak Viscous Action

Bernhard Scheichl*

Institute of Fluid Mechanics and Heat Transfer, TU Wien, Vienna, Austria
AC2T research GmbH (Austrian Excellence Center for Tribology), Wiener Neustadt, Austria

Abstract We exemplify the rigorous treatment of capillarity-driven free-surface flows by considering the “teapot effect” as an appealing daily-life phenomenon. To this end, we formulate the problem in full, elucidate its structure for small viscous influence in a first step and then refine the results by scrutinising the underlying potential flow in due detail. Finally, we address the subtleties arising when it comes to the rational inclusion of viscous effects so as to sort the real flow out of a one-parametric class of inviscid-flow solutions (so-called selection problem). This approach shall demonstrate the successful, systematic treatment of complex flow problems, involving a variety of disparate length scales. Amongst others, it is demonstrated how the correctly performed abstraction process can unveil unexpected mechanisms and deepen the understanding of known physical phenomena. Many intriguing questions associated with the effect in focus are found as not settled conclusively yet. This calls for further analytical and numerical progress.

1 Basic Remarks

These lecture units shall provide an outlook on asymptotic methods and the associated analytical/numerical techniques commonly used to solve the arising reduced problems. These are made explicit by scrutinising in due depth the so-called teapot effect. Specific emphasis is laid on the different spatial scales emerging in the course of its analysis. Definite references for further reading are the classical textbooks by [Van Dyke \(1975\)](#) (matched asymptotic expansions, local solutions, potential flow around a wedge) and [Vanden-Broeck \(2010\)](#) (potential free-surface flows, vanishingly small surface tension, provoking selection problems).

Systematic modelling the teapot effect is archetypical for the application of the KISS principle in science, where KISS is an acronym for “Keep it simple, stupid!”. This is also often referred to as the law of parsimony or *Ockham’s razor*. That is, any empiricism that has formed an input in previous theories but proves superfluous in the end should be avoided. As a general rule, first the essential key groups and their (relative) order of magnitude have to be established by dimensional analysis. Very small/large parameters then lay the basis for the application of perturbation methods as the means of choice when it comes to the rigorous treatment of the phenomenon in question for gaining a

*Email: bernhard.scheichl@tuwien.ac.at. © Bernhard Scheichl, 2023. All rights reserved.

systematic, deep insight into the physics at play. Specifically, the intricate results obtained by the (very scarce) full computational investigations of the teapot effect (Kistler & Scriven, 1994) suggest this approach all the more, for this but also related problems.

These lecture notes aim at providing a flavour of the individual topics and the breadth and variety of the recent and ongoing research.

2 Motivation: The Teapot Effect (and its Prevention)

The teapot effect commonly refers to the tendency of the flow of a liquid layer, essentially driven by inertia and capillary effects, to stay attached to a convex wall (which is obviously undesired when it comes to pouring tea from a spout). Its first phenomenological description of the teapot effect must be attributed to Reiner (1956) (see also Walker, 1984). It becomes evident from his observations that gravity is not crucially at play, but inertial and capillary effects.

Gravity being the typical body force is excluded at the outset: in accordance with the aforementioned empirical findings, its effect appears to be sufficiently weak under usual circumstances, and its inclusion would not alter the main physical consequences but apparently prevent the formation of a developed free jet and thus overcomplicate our analysis. Also, it is known from the asymptotic analysis of thin layers passing sharp to curved (thus nose-type) trailing edges of a horizontal plate that the emerging hydrostatic pressure gradient upstream of the edge provokes complex short-scale breakdowns (viscous–inviscid interaction, see Gajjar, 1987; Higuera, 1994; Scheichl, Bowles & Pasias, 2018, 2021) of the conventional hierarchical asymptotic structure of the flow, as described by matched asymptotic expansions and targeted here throughout.

Assuming a slender layer of liquid passing the lip-type edge of an otherwise flat rigid wall (lip of a spout) models the teapot effect. A crucial ingredient is the strong convex contour of the upside of the lip, possibly followed by concave downside. The three main states of the flow are as follows (see figures 1a–c): a nominally stationary, fully contiguous liquid film detaching from the wall; the limiting situation where the hydrodynamic retention force just impedes its detachment; the break-up of the film due to the pinch-off of droplets, associated with local unsteadiness, as capillary effects overcome the retention force to prevent the flow from following the wall any longer. For the realisation of these phenomena we refer to Duez et al. (2010), here specifically to figure 1(d), and the movie illustrating a series of recent experiments at and made accessible by the TU Wien (2021). We anticipate the consequences inferred from the analytical/numerical findings available: increasing the wall curvature, decreasing the surface tension and decreasing the wettability by decreasing the contact angle between the liquid and the solid wall shifts detachment further upstream and thus weakens the teapot effect.

3 Stating the Problem in Full

For what follows, we tacitly refer to the flow configuration in figure 2 throughout. The abstraction of the problem relies on the following prerequisites. Dimensional quantities shall be indicated by tildes. We consider the

- planar, steady, laminar film of a Newtonian liquid (volumetric flow rate \tilde{Q} per lateral unit depth)

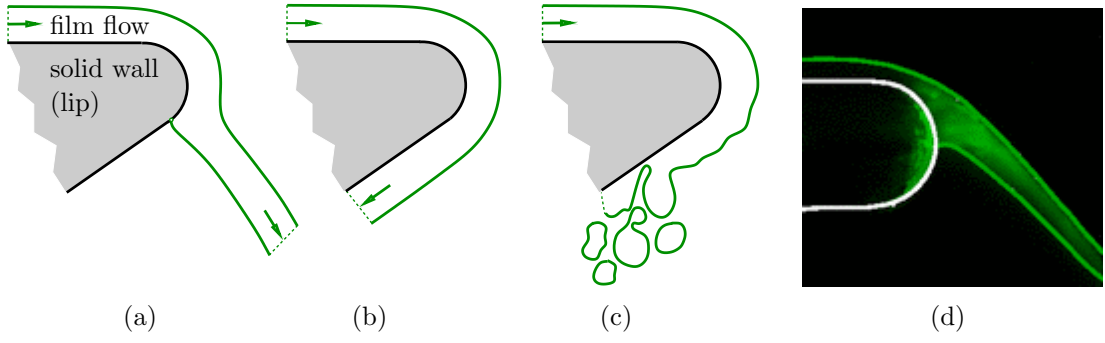


Figure 1: (a)–(c) Sketches of three main manifestations of flow, (d) experimental visualisation of case (a): (a) detachment of film flow from curved wall, (b) flow fully aligned to wall (limiting situation), (c) film rupture and droplet formation; (d) cut of liquid interfaces in experiment, described in and reprinted with permission from [Duez et al. \(2010\)](#) (© American Physical Society).

- over and detaching from a rigid impermeable wall representing the end of the spout and its lip, being perfectly smooth (roughness neglected), possibly apart from an isolated kink (wedge-shaped lip),
- experiencing no mass exchange with the surrounding passive gas at rest
- and having uniform fluid and contact properties (density $\tilde{\rho}$, kinematic viscosity $\tilde{\nu}$, surface tension $\tilde{\tau}$, static contact angle θ_c).
- On the length scales considered, any impact of the freely pouring jet is disregarded.
- The wall geometry is described by a maximum of two reference lengths with sufficient accuracy: if exiting, \tilde{R} , typical of the contour of the end portion of the spout or lip around which the flow is considered, e.g. a characteristic radius of its curvature; a horizontal distance $\tilde{L} \gg \tilde{R}$ along which the flow, poured out from the spout, adjusts before it approaches the spout's lip.

3.1 Basic Estimates and Separation of Scales

We first introduce a typical vertical height \tilde{H} of the adjusting, incident fluid film, yet to be specified and also characteristic of the wall-normal thickness of the film bending around the nose. For this regime we focus on, $\tilde{S} = \max(\tilde{H}, \tilde{R})$ serves as a suitable basic length scale. This selection becomes crucial if a nose-like lip assumes the form of an (acute-angled) wedge such that $\tilde{R} \ll \tilde{H}$ and the characteristic length \tilde{R} is eventually absent. In turn, we make the local flow velocity, \mathbf{u} , non-dimensional with $\tilde{U}_S = \tilde{Q}/\tilde{S}$, the streamfunction, ψ , with \tilde{Q} , the local fluid pressure, p , relative to that in the environment with $\tilde{\rho}\tilde{U}_S^2$ and all lengths with \tilde{S} if not stated otherwise below. The key groups (found by dimensional analysis) controlling the problem are a reciprocal Weber number, τ , and a reciprocal Reynolds number, ϵ , where

$$\tau = \tilde{\tau}/(\tilde{\rho}\tilde{U}_S^2\tilde{S}) \geq 0 \quad \text{as} \quad \epsilon = \tilde{\nu}/\tilde{Q} \rightarrow 0. \quad (1)$$

The last assumption expresses the fact that the incident slender flow evolving over the much bigger adjustment length \tilde{L} might already appear as developed due to viscous action. Then the flow we scrutinise represents the localised and essentially inviscid

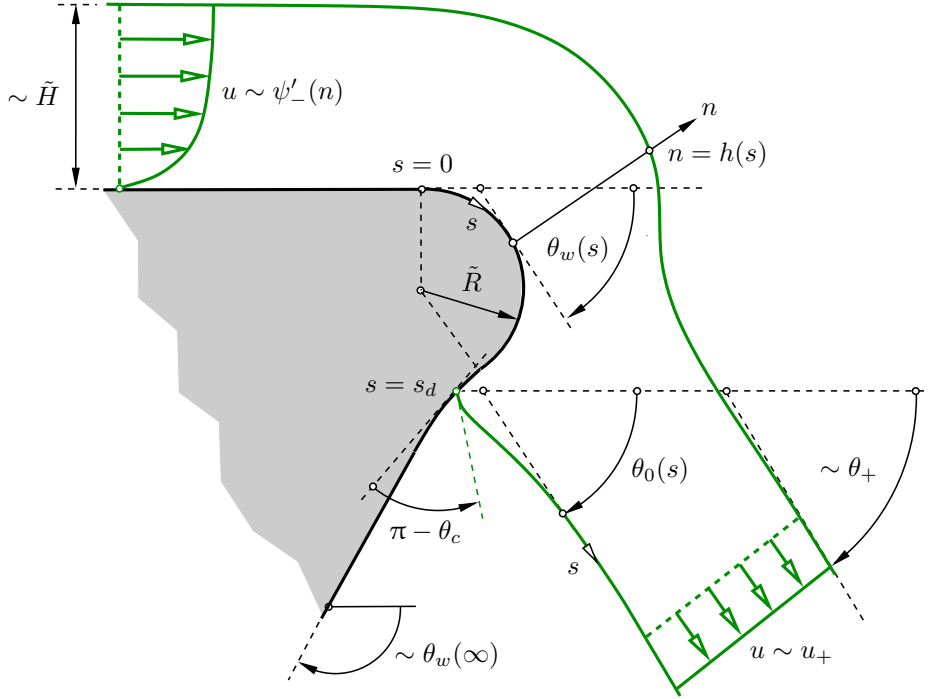


Figure 2: Sketch of flow around lip, not to scale, cf. figure 1.

response due the rather abrupt increase of the wall curvature, expressed by the least-degenerate limit

$$1 \geq H = \tilde{H}/\tilde{S} = O(1) \quad \text{as} \quad L = \tilde{L}/\tilde{S} \rightarrow \infty. \quad (2)$$

We now introduce the effective reference speed $\tilde{U}_H = \tilde{Q}/\tilde{H} = \tilde{U}_S/H$. Let \tilde{n}_ν be the distance from the wall where viscosity is dominantly at play. Since $\tilde{\rho} \tilde{U}_H^2/\tilde{S}$ measures the streamwise fluid acceleration and $\tilde{\rho} \tilde{v} \tilde{U}_H/\tilde{n}_\nu^2$ the transversal shear stress, the dominant momentum balance in that region yields the basic estimate

$$\tilde{U}_H^2/\tilde{S} \sim \tilde{v} \tilde{U}_H/\tilde{n}_\nu^2 = \epsilon (\tilde{U}_H^2/\tilde{H})(\tilde{H}/\tilde{n}_\nu)^2 \quad \text{or} \quad \tilde{n}_\nu/\tilde{H} \sim \sqrt{\epsilon/\tilde{H}}. \quad (3)$$

Therefore, we are principally concerned with two options:

- (i) $H = O(\epsilon)$: slender developed flow around the lip;
- (ii) $H \gg \epsilon$: essentially inviscid core flow, driving a boundary layer (BL) of relative thickness $\sqrt{\epsilon/\tilde{H}}$ adjacent to the wall of the lip.

Here we discard the simplifications the slender-layer approximation in the less feasible scenario (i) implies, in favour of the richer physics and more intriguing results deduced from the situation (ii), which is entailed by (1) and (2). A distance of about \tilde{L} upstream of the lip, the momentum balance for the streamwise direction $\tilde{U}_H^2/\tilde{L} \sim \tilde{v} \tilde{U}_H/\tilde{H}^2 = \epsilon \tilde{U}_H^2/\tilde{H}$ gives

$$L = H/\epsilon \gg 1/\sqrt{\epsilon}. \quad (4)$$

With \tilde{v} , \tilde{Q} , $\tilde{S} \geq \tilde{H}$ and \tilde{L} prescribed, this completes the scaling of the flow. The benefit of the uniform uniform scaling in all directions as \tilde{S} rather than \tilde{H} measures the thickness of the bending film outperforms the disadvantage of an by a factor H effectively much smaller thickness if $1 \gg H \gg \sqrt{\epsilon}$. The factor H enters the leading-order matching of

the slender incident and strongly turning flow (§ 3.4.1), where it accordingly compresses the layer height and flow component in the n -direction but increases the streamwise one. Accordingly, taking \tilde{U}_H as the reference speed for the latter and rescaling the cross-stream by the factor H replaces τ and ϵ by $\tilde{\tau}\tilde{H}/(\tilde{\rho}\tilde{U}_H^2\tilde{S}^2) = \tau H^3$ and $\tilde{\nu}\tilde{S}/(\tilde{U}_H\tilde{H}^2) = \epsilon/H$. Scenario (i) eventually supersedes the present one (ii) and the associated scale separation if H becomes as small as ϵ and, see (4), \tilde{L} indistinguishable from \tilde{S} .

The impact of gravity on the flow is now estimated correctly on the basis of this rescaled inverse Weber number and the corresponding reciprocal squared Froude number $g = \tilde{g}\tilde{H}/\tilde{U}_H^2$ where $\tilde{g} \approx 9.81$ m/s is the gravitational acceleration. Then the Bond number given by their ratio

$$Bo = g/(H^3\tau) = \tilde{\rho}\tilde{g}\tilde{S}^2/\tilde{\tau} \quad (5)$$

(independent of \tilde{H}) serves to measure the influence of gravity relative to that of surface tension. Considering an aqueous liquid at standard conditions and a typical lip of a spout of teapot, we find $\rho \approx 10^3$ kg/m³, $\tau \approx 0.007$ N/m and take \tilde{S} and \tilde{H} as of about 1 mm. As a result, $Bo \approx 0.140$, which is sufficiently small to neglect gravity given other simplifications made. However, the relatively high sensitivity of Bo against the curvature or sharpness of the lip is noticeable.

It proves instructive to first address the viscous free-surface flow problem in its most general form subject to (2) before the reduced inviscid one (§ 5). To this end, we first take ϵ as finite.

3.2 Governing Equations

We conveniently introduce curvilinear coordinates s and n respectively along and perpendicular from the lowermost streamline towards the flow and the associated unit vectors $\mathbf{s}(s)$ in the s - and $\mathbf{n}_0(s)$ in the n -direction. The origin $(s, n) = (0, 0)$ shall designate the onset of the marked wall curvature, $\kappa_w(s)$, for $s > 0$ and thus the the spout lip. It is noted that $\kappa_w > 0$ for a convex wall and thus typical of the upside of the lip. Let $h(s)$ denote the normal distance of the uppermost, entirely free streamline ($\psi = 1$) from the lowermost one (wall and lower free surface, $\psi = n = 0$). Moreover, $\theta(s, n)$ is the flow angle measured in clockwise direction from the horizontal axis, $\theta_0(s) = \theta(s, 0)$ then the inclination angle of the lowermost streamline, $\kappa_0(s) = \theta'_0$ its curvature and $\kappa_1(s)$ that of the upper free one. Likewise, $\theta_0(s)$ equals some $\theta_w(s)$ with $\kappa = \theta'_w$ along the wall. Furthermore, $\partial_s(\mathbf{s}, \mathbf{n}_0) = (-\mathbf{n}_0, \mathbf{s})\kappa_0$ and, in turn, $\nabla = \mathbf{s}l^{-1}\partial_s + \mathbf{n}_0\partial_n$ where

$$l(s, n) = 1 + \kappa_0(s)n \quad (6)$$

is the Lamé coefficient of that natural metric. The curvature κ_1 is given by $\nabla \cdot \mathbf{n}_1(s)$ on $\psi = 1$ where \mathbf{n}_1 is the outer unit normal on this. With $\mathbf{s} + (\mathbf{n}_0 h)' = \mathbf{s}l(s, h) + \mathbf{n}_0 h'$ being the corresponding tangent, we obtain

$$\mathbf{n}_1 = \frac{\mathbf{n}_0 l_1 - \mathbf{s}h'}{(l_1^2 + h'^2)^{1/2}}, \quad \kappa_1(s) = \frac{\kappa_0(l_1^2 + 2h'^2) + \kappa'_0 h' h - h'' l_1}{(l_1^2 + h'^2)^{3/2}}, \quad l_1(s) = l(s, h(s)). \quad (7)$$

We take $[\mathbf{u}, \psi, p] = [\mathbf{u}, \psi, p](s, n)$ and decompose $\mathbf{u} = \mathbf{s}u(s, n) + \mathbf{n}_0 v(s, n)$ to introduce the orthogonal flow components u and v . Then the continuity equation $\nabla \cdot \mathbf{u} = u_s + (lv)_n = 0$ is satisfied identically provided $(u, v) = (\psi_n, -\psi_s/l)$. The convective operator and the Laplacian then read explicitly

$$\mathbf{u} \cdot \nabla = l^{-1}(\psi_n \partial_s - \psi_s \partial_n), \quad \Delta = \nabla^2 = l^{-1}[\partial_s(l^{-1}\partial_s) + \partial_n(l\partial_n)]. \quad (8)$$

We also introduce the dimensionless tensor $\boldsymbol{\Sigma} = \nabla \mathbf{u} + (\nabla \mathbf{u})^T$ of the viscous Cauchy stresses. Hence, $\nabla \cdot \boldsymbol{\Sigma} = \Delta \mathbf{u}$ and $\Delta \mathbf{u} = \Delta \nabla^\perp \psi = \nabla^\perp \Delta \psi$ as $\nabla^\perp = \mathbf{s} \partial_n - \mathbf{n}_0 l^{-1} \partial_s$ is the conjugate gradient. We thereby arrive at the projections of the Navier–Stokes (NS) equations $\mathbf{u} \cdot \nabla \mathbf{u} = -\nabla p + \epsilon \Delta \mathbf{u}$ onto the s - and the n -direction respectively

$$l^2 \mathbf{u} \cdot \nabla \psi_n - \kappa_0 \psi_n \psi_s = -l p_s + \epsilon l^2 \partial_n \Delta \psi, \quad (9)$$

$$l \mathbf{u} \cdot \nabla (-l^{-1} \psi_s) - \kappa_0 \psi_n^2 = -l p_n - \epsilon \partial_s \Delta \psi. \quad (10)$$

The terms proportional to κ_0 herein express respectively the Coriolis and the centripetal accelerations of a fluid particle when viewed in a frame of reference moving with $\mathbf{s} u$ along the lowermost streamline. As seen from (10), a positive curvature generates a positive pressure gradient normal from the wall and thus a tendency of the flow to cling to a convex wall contour. This essential, inertial ingredient to the teapot effect is sometimes also referred to as the ‘‘Coandă effect’’ (see e.g. Guyon et al., 2012, chap. 5.3.3). Eliminating p in (9) and (10) with the aid of (8) recovers, after some rearrangements, the vorticity transport equation

$$\mathbf{u} \cdot \nabla \omega = \epsilon \Delta \omega, \quad \omega = -\Delta \psi \quad (11)$$

is the scalar vorticity.

Boundary conditions (BCs) have to be met on the lower- and the uppermost streamline. The kinematic BCs consist of the aforementioned ones and the usual no-slip condition on the wall,

$$\psi(s, h(s)) = 1, \quad \psi(s, 0) = 0, \quad s \leq s_d: \quad \psi_n(s, 0) = 0, \quad \theta_0(s) = \theta_w(s). \quad (12)$$

Here we have introduced the position $s = s_d$ of dewetting or flow detachment from the wall (if it exists, i.e. the flow detaches at all). In continuum mechanics, the wetting angle θ_c satisfies the well-known Young–Dupré equation over an arbitrarily small length scale. Since this three-phases equilibrium is unaffected by the flow, the following complementary jump condition fixes the detachment angle θ_d formed between the wetted wall and the just generated lower free streamline and finally s_d :

$$\theta_w(s_d-) - \theta_0(s_d+) = \pi - \theta_d, \quad \theta_c \leq \theta_d \leq \theta_c + \theta_w(s_d+) - \theta_w(s_d-). \quad (13)$$

The inequalities herein express the Gibbs inequality in their correct form (see Dyson, 1988; Kistler & Scriven, 1994) and hold if the wall contour exhibits a kink (as does the wedge-shaped lip) at $s = s_d$ such that $\theta_w(s_d+) > \theta_w(s_d-)$. (It is noteworthy that this inequality is a purely geometrical result if that apex is obtained in the limit of a vanishing radius of curvature.) The conventional dynamic BCs express the stress equilibrium the liquid–gas interfaces are subjected to: the total stresses acting on the lower and upper one given by $\epsilon \mathbf{n}_{0,1} \cdot \boldsymbol{\Sigma} - \mathbf{n}_{0,1} p$ must equal $-\mathbf{n}_{0,1} p_{L,0,1}$ where $p_{L,0} = -\tau \kappa_0$ and $p_{L,1} = \tau \kappa_1$ are the corresponding Laplace pressures. Hence, for

$$n = 0, \quad s > s_d: \quad \epsilon \mathbf{n}_0 \cdot \boldsymbol{\Sigma} = \mathbf{n}_0(p + \tau \kappa_0), \quad n = h(s): \quad \epsilon \mathbf{n}_1 \cdot \boldsymbol{\Sigma} = \mathbf{n}_1(p - \tau \kappa_1). \quad (14)$$

These dynamic BCs describe a free-slip condition in terms of requiring zero tangential stress and account for the capillarity-induced normal-stress jump. There is no need to state $\boldsymbol{\Sigma}$ in (14) explicitly, upon execution of ∇ and substitution of (7), in the light of the subsequent investigation.

Given the definition of \tilde{H} , h stays finite as $s \rightarrow -\infty$. Hence, our concern is with the far-upstream matching conditions

$$h(-\infty) = h_-, \quad \psi(-\infty, n) = \psi_-(n) \quad (15)$$

where the value of h_- and the profile ψ_- of the incident flow are given. However, they are yet to be determined by envisaging the flow taking place over the horizontal extent L , see (2). The no-slip condition requires the regular behaviour $\psi'_- = O(n)$ ($n \rightarrow 0$). Arbitrarily far downstream, a physically admissible free jet must not intersect itself. This topological constraint requires the streamline curvature and thus $\kappa_{0,1}$ to vanish for $s \rightarrow \infty$ as for $s \rightarrow -\infty$. We anticipate that a uniform parallel flow describes the terminal structure of the jet as the vorticity dies out by the action of viscous diffusion. In combination with the outflow or forward-flow condition, it is indeed sufficient to require

$$h'(\infty) = \theta'_0(\infty) = 0, \quad \psi_n(\infty, n) > 0. \quad (16)$$

Tied in with (15) and (16), $p \rightarrow 0$ as the film (upstream) and jet (downstream) become slender. These BCs complete the formulation of the flow problem, consisting of (9) and (10) supplemented with (6)–(8) and subject to (12)–(16) as governing $[\psi, p](s, n)$, $h(s)$, s_d , $\theta_0(s)$, this for $s > s_d$. The specification of h_- and ψ_- as well as the rationale underlying (16) are deferred to §3.4.

One has to be aware of that for $|s|$ becoming large, as the free streamlines become straight lines, the capillary influence is manifest as surface ripples having a wavelength comparable to H and dying out exponentially: cf. Scheichl, Bowles & Pasias (2018) for the upstream and Scheichl, Bowles & Pasias (2021) for the downstream case. Tied in with the well-posedness of the problem, this behaviour provides the excitation of non-trivial values of h' as $s \rightarrow \pm\infty$ and θ_0 as $s \rightarrow +\infty$ because h' , h'' and θ'_0 enter the problem via (7) and (14). The terminal thickness and uniform speed of the pouring jet, $h_+ = h(\infty)$ and $u_+ = u(\infty, n)$, are then determined by h_- , ψ_- and global conservation of linear momentum and the volume flow ($h_+u_+ = 1$).

3.3 Essential Preliminary Findings

Even without knowing the parametrised solution to the full NS problem stated above, one can deduce some of its most important properties from previous related studies and the inviscid limit. We list these in the following.

- As indicated by the last considerations closing §3.2, the uniform terminal turning angle of the jet, $\theta_+ = \theta(\infty, n)$, is part of the solution. On geometrical grounds, $0 \leq \theta_+ \leq \max \theta_w = \theta_w(\infty) \leq \pi$. This is the state referred to by figure 1(b).
- The wavelengths of the decaying short-scale capillary undulations above the wall far upstream and on two free surfaces far downstream are typically controlled by Rayleigh problems of free-surface type (Scheichl, Bowles & Pasias, 2018, 2021). However, this local, inviscid description should be complemented by the streamwise modulation of their wavelength and the attenuation of their amplitude found by a (yet unavailable) WKB (Wentzel–Kramers–Brillouin–Jeffreys) analysis. This correctly accounts for the slowly varying background flow as $[\psi, h] \rightarrow [\psi_{\pm}, h_{\pm}]$.
- The analysis in the inviscid limit $\epsilon = 0$ (§5) reveals a loss of the existence of the solution to the steady-state problem if the value of τ exceeds some critical threshold $\tau^*(\theta_c, \epsilon)$, where $\theta_+ = \max \theta_w$ for a fixed wall geometry. This is a central result of

the (non-rigorous) investigation of the integral conservation of linear momentum where the hydrodynamic retention force caused by the suction pressure near the tip or highest curvature of the lip must be modelled (Duez et al., 2010; Bouwhuis & Snoeijer, 2015, unpublished).

- This loss suggests an appealing physical interpretation: presumably, it corresponds to incipient break-up of the film into droplets and a fully trickling behaviour as the flow can neither cling to nor detach from the wall any longer.
- Finally, the momentum balance for the inviscid flow as well as the asymptotic analysis by Scheichl, Bowles & Pasias (2021) of a developed flow passing a relatively sharp lip indicate the following trends: a higher wettability of the wall, i.e. increasing θ_c , increases θ_+ and thus promotes the teapot effect; the same trend is found for increasing τ ; however, the associated behaviour of s_d exhibits a non-uniqueness with respect to the variation of τ ; increasing the sharpness of the lip (such that \tilde{S} becomes \tilde{H}) tentatively suggests a decrease of the pressure force and therefore a contrary tendency; also, both increasing θ_c and the curvature of the lip shifts τ^* to larger values and thus stalls the onset of trickling.

As a highlight of their study of the global momentum balance, Bouwhuis & Snoeijer (2015) predict an absolute minimum of τ for which the fully attached film can bend around a lip having the shape of a semi-circle $\theta_c = \pi$ but is on the verge of trickling. Under their restriction of an irrotational flow ($u_- = u_+ = 1$),

$$\min \tau(\theta_c, 0) = \tau^*(\pi, 0) = 1/2 \quad \text{for} \quad \theta_+ = \pi. \quad (17)$$

As the authors noticed, then \tilde{U} just equals the well-known Taylor–Culick (TC) speed of a retracting inviscid thin sheet: as demonstrated by Taylor (1959b) and Culick (1960), in a first approximation, the temporal change of the momentum contained in the “blob” forming at the end of the sheet equals the surface force drawing on it (alike an extreme localised Marangoni effect). This gives, in our notation, $\tilde{U} = [2\tilde{\tau}/(\tilde{\rho}\tilde{H})]^{1/2}$ for that speed. Likewise, in the present scenario the film starts to disintegrate once its momentum flow per unit depth is exactly compensated by surface tension as the hydrodynamic retention (pressure) force vanishes. For $\tau > 1/2$, the film has ruptured due to droplet formation. Our preliminary investigation shows that this critical threshold stays intact under the more realistic assumption of vorticity being carried in by the (developed) flow upstream, which corroborates its physical interpretation. More generally, we find

$$T = \frac{\tau}{J} < \frac{1}{2}, \quad J = \int_0^{h^-} \psi_-'^2(n) \, dn, \quad (18)$$

for the reciprocal Weber number T suitably formed with the incoming momentum flow J . It is an unsettled question how finite values of ϵ modify this constraint.

Solving the full problem poses a formidable numerical challenge, given the initially unknown positions of the two free streamlines, including origin $(s, n) = (s_d, 0)$ of the lower one. Mastering it longs for the transformation $\eta = n/h(s)$, mapping the physical plane onto the unit stripe $-\infty < s < \infty$, $0 \leq \eta \leq 1$. To the author’s knowledge, the only available relevant solution is by Kistler & Scriven (1994), who considered the flow past an acute wedge by including gravity, adopting some further simplifications and using finite elements. Their variation of the Reynolds number, the characteristic Kapitza number and θ_c confirms the trends mentioned above even though embedded in a surprising complexity and non-uniqueness of the flow, involving localised reversed-flow

eddies immediately upstream of flow detachment. Experiments carried out by these authors corroborate their numerical findings. However, their variety still longs for a clarification by asymptotic analysis.

3.4 Far-Upstream and -Downstream Conditions

We now address the missing ingredients leading to (15) and (16) with due rigour. These concern special self-similar solutions of the NS equations and their reduction to the slender-flow and BL equations.

3.4.1 Far Upstream: Watson's Flow Revisited

In the distinguished developed-flow limit given by (1) and (4), we describe the oncoming flow over the almost horizontal part of the wall (spout) upstream of its lip by setting $x = s/L = O(1)$ ($x \leq 0$) and writing $[\psi, h/H] \sim [f(x, \eta), h_u(x)] = O(1)$. To leading order, f and h_u satisfy the slender-layer approximation of (9) subject to (12) and the free-slip condition at the free surface arising from (14) while (10) predicts $|p|$ being as small as τ/L^2 . By the change of variables,

$$h_u(f_\eta f_{\eta x} - f_x f_{\eta\eta}) - h'_u f_{\eta\eta}^2 = f_{\eta\eta\eta}, \quad (19)$$

$$\eta = 0: \quad f = f_\eta = 0, \quad \eta = 1: \quad f = 1, \quad f_{\eta\eta} = 0. \quad (20)$$

Formulating appropriate upstream conditions, modelling the generation of the flow at the virtual origin $x = -1$ (i.e. the end of the spout), complements (19) and (20) to a parabolic problem governing f and h_u , to be solved via numerical downstream marching. Matching provides $\psi_-(n)$ and h_- as given by the terminal values $f(0, \eta)$ and $Hh_u(0)$.

It deserves mentioning at this point that typically the Mangler–Stepanov transformation can be used to convert the solution of the above problem into that governing the streamfunction f of the corresponding axisymmetric radial flow: then $\rho = (3x)^{1/3}$ is the radial distance from the axis, $h_u(x)/\rho$ the film height, thus $\eta h_u/\rho$ the axial flow position.

In many related situations, L is so large that the flow described by f and h_u can be regarded as almost fully developed or independent of its upstream history. This probably not applies to the rationally founded description of the flow emitted by a spout, but the associated universality of ψ_- and h_- is beneficial and provides a good qualitative approximation of more realistic upstream conditions even though. One readily finds that $f \sim f_W(\eta)$ and $h_u \sim a_W(x + 1)$ with $a_W = \text{const}$ expresses this self-preserving state of the flow as $-a_W f_W'^2 = f_W'''$ where a_W represents an eigenvalue. This special flow was investigated first by Watson (1964). Notably, f_W' can be expressed by a Jacobi elliptic function, and $a_W = \pi/3^{1/2}$.

Given the the linear growth of $h_u(x)$, Watson's planar flow is unaffected by surface tension for howsoever large values of τ (in contrast to its axisymmetric counterpart, where the film height increases quadratically with the radius).

3.4.2 Far Downstream: Squire–Taylor Modes Over Uniform Flow

In general, the nearly straight streamlines sufficiently far downstream represent a source flow with some opening angle 2α greater or, in the case of a parallel flow, equal to zero and smaller than 2π . It is expedient at this point, also for later purposes, to introduce polar coordinates: the radial distance r measured from the centre assumed in some point of the lower free streamline; the azimuth angle φ measured in counterclockwise direction

from the latter. By the local absence of a characteristic length scale, we seek ψ and p typically via separation of variables involving (logarithmic–)algebraically varying gauge functions in r in the form

$$\psi \sim r^\lambda F(\varphi), \quad p - p_0 \sim r^{\lambda-2} \Pi(\theta), \quad (21)$$

where the radial pressure variation is replaced by $\ln r$ if $\lambda = 2$ either for $r \rightarrow \infty$ or $r \rightarrow 0$ for any finite, however small value of ϵ . The constant λ and F , Π (parametrised by ϵ) are determined in the course of the analysis. The variation of p in (21) follows from (9) and (10), where p_0 denotes some constant of integration and we tacitly include a logarithmic radial variation if $\lambda = 2$. With the unit vectors \mathbf{e}_r in the radial and \mathbf{e}_φ in the azimuthal direction, $\nabla = \mathbf{e}_r \partial_r + r^{-1} \mathbf{e}_\varphi \partial_\varphi$, and one finds the corresponding components Σ_{ij} ($i, j = r, \varphi$) of Σ as given by

$$\frac{\Sigma_{rr}}{r^{\lambda-2}} = 2[(\lambda-1)F' + \lambda r F], \quad \frac{\Sigma_{r\varphi}}{r^{\lambda-2}} = F'' + \lambda(2-\lambda)F, \quad \frac{\Sigma_{\varphi\varphi}}{r^{\lambda-2}} = 2(1-\lambda)F'. \quad (22)$$

Specifically, here continuity implies $|\mathbf{u}| = O(1/s)$ for $s \rightarrow \infty$, subject to (12). Let the polar centre coincide with the virtual intersection of the free streamlines. We then have $\psi \rightarrow F$ ($0 \leq \varphi \leq \alpha$, $\lambda = 0$) as $r \rightarrow \infty$, i.e. the flow assumes a special member of the class of the well-known self-preserving Jeffery–Hamel (JH) flows (Fraenkel & Squire, 1962). Restricted to a purely radial forward flow, this is seen as the half of a symmetric jet. The NS equations for the radial and azimuthal directions and (11) become respectively

$$\Pi = -(F'^2 + \epsilon F''')/2, \quad \Pi' = 2\epsilon F'', \quad \epsilon(F'' + 4F)' + F'^2 + 2C = 0 \quad (23)$$

with some integration constant C . Accordingly, (12) entails $F(0) = 0$, $F(\alpha) = 1$ and (14), in combination with (22) and $\mathbf{n}_{0,1}$ identified with \mathbf{e}_φ , $F''(0) = F''(\alpha) = 0$, $2\epsilon F'(\alpha) = \Pi(\alpha)$, so this condition $C = 0$. Then the last equation in (23) subject to the remaining four BCs represents an eigenvalue problem for F and positive eigenvalues of α . However, the contradiction $\int_0^\alpha F'^2 d\varphi = -4\epsilon$ stymies their existence. (We note that (23) recovers the classical radial irrotational flow as $F' = 1/(2\pi)$, which, however, requires the absence of free streamlines and thus $\alpha = 2\pi$.)

We are thus left with the only possibility of a parallel, developed flow, where (9) yields $\psi_{nn} = 0$. Then the BCs confirm the uniform plug flow, $u = u_+$. It is interesting to focus on the aforementioned capillary undulations of accordingly damped amplitude on a streamwise scale comparable to the terminal jet height $h_+ = 1/u_+$: these then are stationary Squire–Taylor modes (Squire, 1953; Taylor, 1959a; Drazin & Reid, 2004, chap. 1). The two families of linear harmonic modes are depicted in figure 3(a): “flapping”, sinusoidal or symmetric ones; “varicose” or anti-symmetric ones. Their phase speeds c_+ and wavenumbers k_+ , non-dimensional with $u_+ \tilde{U}_S$ and $h_+ \tilde{S}$, found by normal-mode analysis satisfy the dispersion relations

$$(c_+ - 1)^2 = \tau h_+ k_+ \times \begin{cases} \coth(k_+/2) & \text{(skew-symmetric modes),} \\ \tanh(k_+/2) & \text{(symmetric modes).} \end{cases} \quad (24)$$

These recover the classical anomalous dispersion of capillary waves. Here our concern is with $c_+ = 0$, which yields the constraints between $\tau_+ = \tau h_+$ and k_+ maintaining steady wavetrains, plotted in figure 3(b). The decrease of the actual dimensionless surface tension τh_+ with k_+ can be explained by surface tension balancing the integral momentum flux at two vertical cuts through the layer a wavelength apart. For symmetric

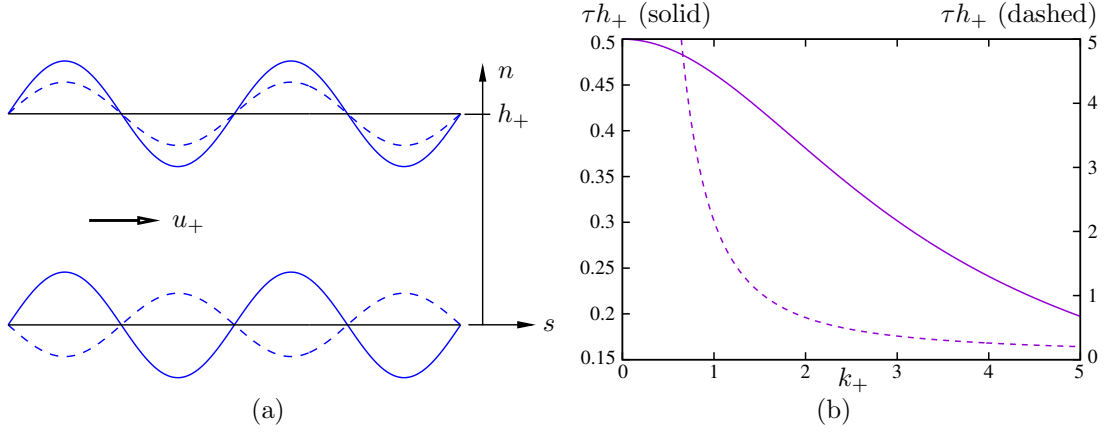


Figure 3: Stationary antisymmetric (solid) and symmetric (dashed) Squire–Taylor modes over locally unperturbed uniform flow: (a) sketch; (b) τh_+ vs. k_+ by (24) with $c_+ = 0$.

waves, where the perturbed streamlines are anti-parallel, higher values of τ_+ compensate for the with decreasing values of k_+ reduced inclination of the streamlines, finally leading to the pole emerging in the long-wave limit $k_+ \rightarrow 0$; for the antisymmetric ones, where the streamlines are parallel, the momentum flow can again no longer sustain the drawing surface force once the terminal flow speed becomes as small as the TC speed or $\tau_+ \rightarrow 1/2-$ as $k_+ \rightarrow 0$, in full agreement with the findings of the strongly nonlinear analysis summarised in §3.3.

4 Weakly Perturbed Stokes Flow Near Detachment

The flow near detachment represents an essential ingredient to the full solution. According to (13), break-away is locally described by a wedge flow of turning angle θ_d , where the wedge is formed by wall upstream ($s < s_d$) and by the lower free streamlines downstream ($s > x s_d$) of the detachment point. The flow variables then again admit the form (21), where the centre of the polar coordinates now lies in the detachment point as we take $r \rightarrow 0$.

We make the dependence of F , Π on ϵ explicit by assuming

$$F \sim \gamma(\epsilon)F_0(\varphi), \quad \Pi \sim \epsilon\gamma(\epsilon)\Pi_0(\varphi) \quad (\epsilon \rightarrow 0) \quad (25)$$

for some gauge function $\gamma > 0$ and $F_0, \Pi_0 = O(1)$ In general, here the offset pressure p_0 must be taken as finite as $\epsilon \rightarrow 0$. Then (22) giving $\epsilon\Sigma = O(\epsilon\gamma r^{\lambda-2})$ confirms that the viscous stresses scale with $p - p_0$. We impose three further constraints:

$$(I) \quad 0 < \theta_d < \pi, \quad (II) \quad \text{Re } \lambda > 1, \quad (III) \quad r \ll \rho(\epsilon) = [\epsilon/\gamma(\epsilon)]^{1/\text{Re } \lambda}. \quad (26)$$

The regular scenario $\theta_d = \theta_c$ demands continuous inclination of the wall in the detachment point such that the wedge filled with liquid is concave. In the remaining pathological situation, the Gibbs inequality allows also for $\theta_d > \pi$. However, detachment from a sharp tip to a wedge apex generally calls for a further inner limit governed by the microscopic length scale characteristic of the then accordingly smoothed apex. We here exclude this degenerate case as well as the hypothetical limit $\theta_c = \pi$ of a perfectly superhydrophobic wall. Restricting the results below to the range (I), see figure 4(a), meets reality if $\theta_d = \theta_c$ but even accounts for the possibility $\theta_c \neq \theta_d < \pi$. The condition

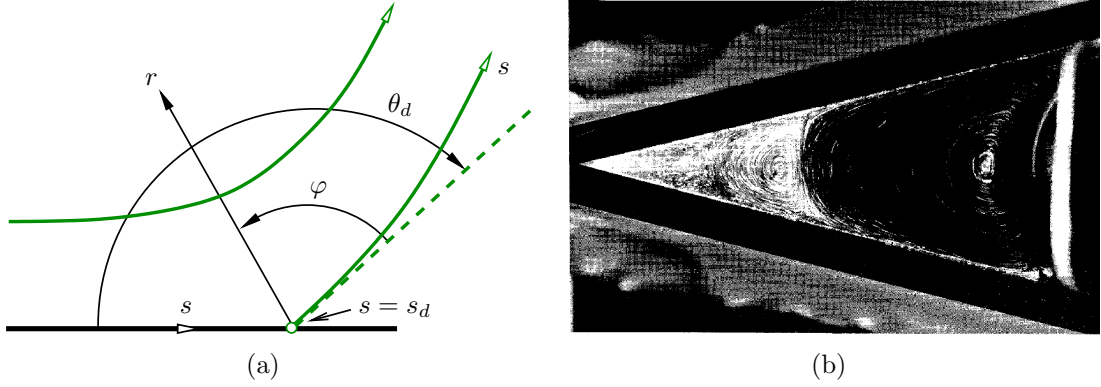


Figure 4: (a) Corner flow immediately near detachment; (b) Photograph of Moffatt's eddies by Taneda (1979) in a roll-driven wedge flow for a characteristic Reynolds number ≈ 0.17 (© Physical Society of Japan).

(II) grants integrability of the stresses being of $O(r^{\lambda-2})$ as $r \rightarrow 0$. Finally, the requirement (III) entails the Stokes limit of (11). At first, analysis by inspection reveals the inertial–viscous balance as retained in full at distances r comparable to $\rho(\epsilon)$ introduced by (III).

The precise form of $\gamma \gg \epsilon$ must be ascertained by matching the associated local NS solution in leading order to the surrounding adjustment of the BL to this wedge-shaped gross break-away of the entire film. However, this would require a thorough but yet unavailable understanding of the multi-tiered splitting of the oncoming BL, due to the contraction of the streamwise scale as $s - s_d \rightarrow 0^-$. Even though, for the time being, one can assure that the polar separation of variables subject to (II) and thus a Stokes limit must take place arbitrarily close to the detachment point.

In leading order, (11) reduces to the biharmonic equation $\Delta^2(r^\lambda F_0) = 0$ subject to (12) for $\varphi = 0$ and θ_d and the free-slip condition by virtue of the requirement of zero tangential stress in (14) implying $\Sigma_{r\varphi} = 0$, see (22). Then the polar decomposition of Δ yields $\omega \sim \gamma r^{\lambda-2} \omega_0(\varphi)$ with ω_0 and F_0 determined by a (self-adjoint) eigenvalue problem with respect to λ as a function θ_d :

$$(\lambda - 2)^2 \omega_0 + \omega_0'' = 0, \quad -\omega_0 = \lambda^2 F_0 + F_0'', \quad F_0(0) = F_0''(0) = F_0(\theta_d) = F_0'(\theta_d) = 0. \quad (27)$$

The eigenfunctions F_0 , proportional to some θ_d -dependent factor determined by the solution to the aforementioned full NS problem, are given by

$$F_0 = \begin{cases} (\sin(\lambda\varphi) \sin[(\lambda - 2)\theta_d] - \sin(\lambda\theta_d) \sin[(\lambda - 2)\varphi]) / (\lambda - 2) & (\lambda \neq 2), \\ \sin(2\varphi) \theta_d - \sin(2\theta_d) \varphi & (\lambda = 2). \end{cases} \quad (28)$$

Factors herein were chosen such that continuity is achieved for $\lambda = 2$. The eigenvalue relation follows from the free-slip condition, i.e. the last BC in (27):

$$(\lambda - 1) \sin(2\theta_d) = \sin[2\theta_d(\lambda - 1)] \quad (\lambda \neq 2), \quad \tan(2\theta_d) = 2\theta_d \quad (\lambda = 2). \quad (29)$$

The branches of (29) were discussed first in the study of corner flows by Moffatt (1964) and taken up in more depth by Scheichl, Bowles & Pasias (2021). Here we resume this analysis to extend the previous results. For their following summary we refer to figures 4(b) and 5:

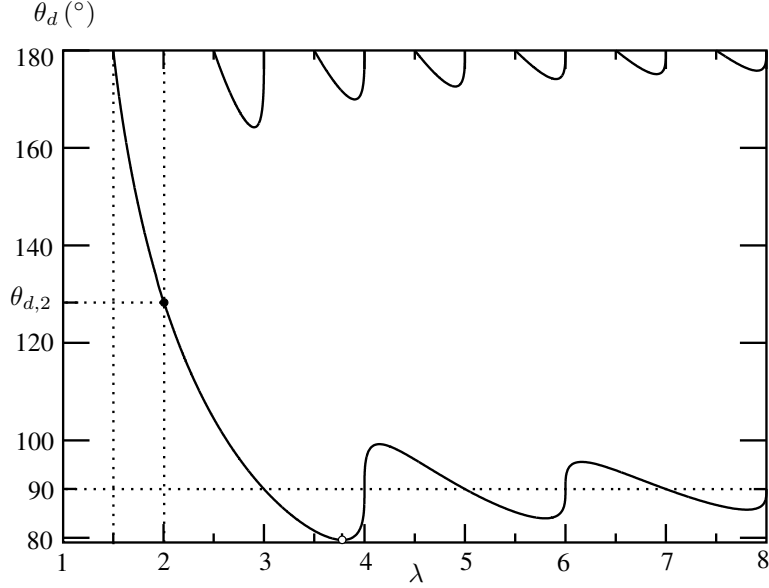


Figure 5: Static contact angle θ_d vs. λ (cases $\lambda = 2$ and $\lambda = \lambda^*$ highlighted).

- The real branches of θ_d as function of λ exhibit an absolute minimum at the turning point $\lambda = \lambda^* \approx 3.7818$, $\theta_d = \theta_d^* \approx 79.557^\circ$. For smaller wetting angles, $\text{Im } \lambda \neq 0$ predicts a family of the infinite, radially aligned sequence of Moffat's celebrated eddies, where $\text{Re } \lambda$ controls their (numerically rather large) damping rate (Moffatt, 1964). As this flow picture can hardly be accepted as a physically viable solution, θ_d falling below of θ_d^* is presumably associated with a loss of stationarity. However, this situation is yet to be clarified.
- A discrete set of real eigenvalues of cardinality ≥ 2 is found for values of θ_d between θ_d^* and $\theta_d^- \approx 100^\circ$ and between $\theta_d^+ \approx 165^\circ$ and 180° . Their number increases to ∞ for $\theta = 90^\circ$ ($\lambda = 3, 4, 5, \dots$) and in the fully hydrophobic limit $\theta_c = 180^\circ$ ($\lambda = 3/2, 4/2, 5/2, \dots$).
- For $\theta_d^- < \theta_d < \theta_d^+$, λ is real and unique, where $\theta_d = \theta_{d,2} \approx 128.727^\circ$ applies to the degenerate case $\lambda = 2$.
- Physically admissible solutions must not exhibit gross reversed-flow regions. This applies to all minimum values of $\lambda \in \mathbb{R}$ as $F_0(\varphi) > 0$ for all $\varphi \in (0, \theta_d)$.

We may now formulate the present Stokes limit more precisely. To this end, we consider (11) restored in full by taking

$$\hat{r} = r/\rho(\epsilon) = O(1), \quad [\psi/\epsilon, (\rho/\epsilon)^2(p - p_0)] \rightarrow [\hat{\psi}, \hat{p}](\hat{r}, \varphi) \quad (\epsilon \rightarrow 0). \quad (30)$$

We note that the reference distance ρ is effectively independent of λ but remains undetermined as long as our understanding lacks the BL structure near detachment. The most interesting of the analysis of the complete NS solution expressed via the $O(1)$ -quantities $\hat{\psi}$ and \hat{p} boils down to the small- \hat{r} expansion

$$[\hat{\psi}, \hat{p}]_{\hat{r} \rightarrow 0} = \sum_{i \geq 0} c_i(\theta_c) [\hat{r}^{\lambda_i} F_i(\varphi), \hat{p}_i] + c.c. + c_0^2 \hat{r}^{2\lambda_0} [G_0(\varphi), \hat{r}^{-2} \Gamma_0(\varphi)] + \dots, \quad (31)$$

$$\hat{p}_i = \begin{cases} \hat{r}^{\lambda_i - 2} \Pi_i(\varphi) & (\lambda_0 \neq 2), \\ \ln \hat{r} \Pi_i & (\lambda_0 = 2, \Pi_i = \text{const}), \end{cases} \quad (32)$$

where constants of integration are already absorbed by p_0 . The coefficients c_i are taken as fixed by the full NS solution, and the index $i = 0$ now refers only to the, physically acceptable and most relevant, eigenvalue of smallest real part while the subscripts $i > 0$ indicate the cases exhibiting a multiplicity of λ . Hence, we take $c_0 > 0$ so as to guarantee strict forward flow. The functions G_0, Γ_0 then govern the dominant weak disturbance of the Stokes limit due to its forcing of its inertial response, see (11). They solve the accordingly inhomogeneous counterpart to (27).

The azimuthal pressure variations $\Pi_i(\varphi)$ follow from the Stokes balances

$$\nabla \hat{p}_i = \Delta \mathbf{u}_i, \quad \mathbf{u}_i = \hat{r}^{\lambda_i - 1} (\mathbf{e}_r F'_i - \mathbf{e}_\varphi F_i) \quad (33)$$

are the corresponding velocity contributions. This yields

$$\Pi_i = \begin{cases} \frac{\lambda_i^2 F'_i + F_i'''}{\lambda_i - 2} = \frac{4(1 - \lambda_i) \sin(\lambda_i \theta_c) \cos[(\lambda_i - 2)\varphi]}{\lambda_i - 2} & (\lambda_0 \neq 2), \\ -4 \sin(2\theta_d) & (\lambda_0 = 2). \end{cases} \quad (34)$$

The first of the dynamic BCs (14) in combination with (22) gives the limiting variation of total normal stress $\epsilon \Sigma_{\varphi\varphi} - p$ as

$$\epsilon \Sigma_{\varphi\varphi} - (p - p_0) \underset{\hat{r} \rightarrow 0}{\sim} \frac{\epsilon^2 c_0}{\rho^2} \times \begin{cases} \hat{r}^{\lambda_0 - 2} [(4 - 6\lambda_0 + 3\lambda_0^2) F'_0 + F_0'''] / (2 - \lambda_0) & (\lambda_0 \neq 2), \\ (4 \ln \hat{r} + 1) \sin(2\theta_d) - 2\theta_d \cos(2\varphi) & (\lambda_0 = 2). \end{cases} \quad (35)$$

After some algebra using (28), one then obtains the shape of the just detaching streamline, first for

$$\lambda_0 \neq 2, \quad \Delta s = s - s_d \rightarrow 0+: \quad (36)$$

$$\tau \kappa_0(s) + p_0 \sim \frac{2\epsilon^2}{\rho^{\lambda_0}} \frac{c_0 \lambda_0 (\lambda_0 - 1)}{\lambda_0 - 2} [\sin(\lambda_0 \theta_d) - \sin(\lambda_0 \theta_d - 2\theta_d)] (\Delta s)^{\lambda_0 - 2} + c.c. < 0, \quad (37)$$

$$\theta_0(s) = \theta_w(s_{d-}) - \tau p_0 \Delta s + O(\Delta s^{\lambda_0 - 1}) \quad (\theta_d \neq \pi/2, \pi). \quad (38)$$

Likewise, we have in the special case

$$\lambda_0 = 2, \quad \Delta s / \rho \rightarrow 0+: \quad (39)$$

$$\tau \kappa_0(s) + p_0 \sim (\epsilon / \rho)^2 c_0 [(4 \ln(\Delta s / \rho) + 1) \sin(2\theta_d) - 2\theta_d \cos(2\varphi)] < 0, \quad (40)$$

$$\theta_0(s) = \theta_w(s_{d-}) - \tau p_0 \Delta s + O(\ln(\Delta s / \rho)). \quad (41)$$

These relations prompts us to distinguish between the following cases.

- $\theta_d \geq \theta_{d,2}$ ($\lambda_0 \leq 2$): the diverging normal stress produces a convex underside of the free film at detachment ($\kappa_0 \rightarrow -\infty$ as $\Delta s \rightarrow 0+$), which occurs in an irregular manner. This is the situation sketched in figure 4(a). A higher-order analysis is necessary though in the superhydrophobic limit $\theta_c \rightarrow \pi$ where the right side of (37) vanishes.
- $\theta_d < \theta_{d,2}$ ($\lambda_0 > 2$): detachment is controlled by the (yet unknown) local Laplace pressure p_0 as the viscous normal stress dies out irregularly.

The flow arbitrarily close to detachment is controlled by viscosity (ϵ) and capillarity (τ , θ_c). Here a small viscous length scale is given by ρ and as any non-vanishing p_0 induced by the presence of a BL. In contrast, Moffatt (1964) in his pioneering study considered a Stokes flow from the outset and, therefore, ignored any presence of such a further length scale. Here this situation is recovered by setting γ to unity in (25) and p_0 to zero throughout. Then the scaling factors $\epsilon^2/\rho_0^\lambda$ in (37) and (40) reduce to ϵ , and the capillary number

$$Ca = \epsilon/\tau = \tilde{\rho}\tilde{v}\tilde{U}_S/\tilde{\tau} \quad (42)$$

is the sole dimensionless group locally relevant. Moffatt (1964) also ignored the normal-stress balance at the interface and assumed a wedge flow by disregarding any deviation of the shape of the detaching streamline from a straight line. This is feasible by requiring $Ca \rightarrow 0$: physically, by this predominance of the surface over internal friction force the free streamline acts as a rigid boundary that permits the fluid to slip along it. Apparently, in the opposite case $Ca \rightarrow \infty$ the initial curvature of the free can only be calculated in a suitably defined distinguished superhydrophobic limit $\theta_c \rightarrow \pi$ such that the left and right sides of (37) vanish at the same rate. Remarkably, this restriction proves sensible from a physical point of view: only then the influence of surface tension becomes consistently marginalised in the Young–Dupré equation, balancing the surface tensions of all three phases involved.

Due to the curvature of the free streamline, the inhomogeneities in the problems controlling the convective feedback entering (31) also affect the BCs. Since also $2\lambda_0$ is an eigenvalue in the cases $\theta_d = \pi/2$ and π , further restrictions will arise from the associated solvability conditions. For instance, $\theta_d = \pi$ as $\theta_0 \equiv 0$ for the NS problem over the upper half of the physical plane considered by Scheichl, Bowles & Piasis (2021), but the secularity condition implies $c_0 = 0$.

5 Euler Problem for Non-Zero Vorticity

To address the distinguished limit (1) and (3) and thus the BL structure of the flow properly, one has first to consider the essentially core of the layer occupied by essentially inviscid flow and introduce there uppercase $O(1)$ -quantities for

$$\epsilon \rightarrow 0: \quad [\psi, \omega, \theta, p, |\mathbf{u}|, \mathbf{u}] \rightarrow [\Psi, \Omega, \Theta, P, Q, \mathbf{U}]. \quad (43)$$

Since Ω is conserved along $\Psi = \text{const}$ (and given by $-\psi'_-(n)$ representing the developed incident flow), the natural coordinates are preferably replaced by curvilinear ones along and perpendicular to each streamline. We then adopt Ψ and a pseudo-potential Φ as independent variables, Φ shall equal the flow potential if $\Omega \equiv 0$, and the flow speed Q , the flow angle Θ and the pressure P as dependent ones: $[Q, \Theta, P](\Phi, \Psi)$. The orthogonality relation or set of Beltrami equations are then condensed into

$$\nabla\Phi = \chi(\Phi, \Psi)\nabla^\perp\Psi, \quad \nabla^\perp\Psi = \mathbf{U}. \quad (44)$$

Hence, Φ serves as a progress variable and χ an integrating factor yet to be determined. It shall satisfy $\chi \equiv 1$ in the case of an irrotational flow. With \mathbf{e}_Φ and \mathbf{e}_Ψ being the unit vectors respectively in the Φ - and the Ψ -direction, $(\nabla, \nabla^\perp)\Psi = (\mathbf{e}_\Psi, \mathbf{e}_\Phi)Q$ and $\nabla = Q(\mathbf{e}_\Phi\chi\partial_\Phi + \mathbf{e}_\Psi\partial_\Psi)$. Furthermore, $\partial_{\Phi, \Psi}(\mathbf{e}_\Phi, \mathbf{e}_\Psi) = (-\mathbf{e}_\Psi, \mathbf{e}_\Phi)\Theta_{\Phi, \Psi}$. In turn, $\mathbf{U} \cdot \nabla = \chi Q^2\partial_\Phi$ and $\nabla \cdot \mathbf{U} = \chi Q Q_\Phi - Q^2\Theta_\Psi$.

5.1 Governing equations

On applying the relationships above, we arrive at the Euler equations consisting of the continuity equation (45) and the momentum equations (46) and (47):

$$\chi Q_\Phi - Q\Theta_\Psi = 0, \quad (45)$$

$$QQ_\Phi = -P_\Phi, \quad (46)$$

$$-\chi Q^2\Theta_\Phi = -P_\Psi. \quad (47)$$

Eliminating P confirms that $\Omega = -\Delta\Psi$ is convected along the streamlines and thus just a function of Ψ :

$$\chi Q^2\Theta_\Phi + QQ_\Psi = -\Omega(\Psi). \quad (48)$$

Requiring $\nabla \times \nabla\Phi = \mathbf{0}$ in (44) yields the integrability condition governing χ in differential and integrated form as

$$Q^2\chi_\Psi = \chi\Omega, \quad \chi = \exp \int_1^\Psi \frac{\Omega(t)}{Q^2(\Phi, t)} dt. \quad (49)$$

We adhere to two conventions without any loss of generality: we conveniently set $\chi(\Phi, 1) = 1$; from here onwards, we identify the origin of (Φ, Ψ) with the point of flow detachment. By the first choice, χ exists for $0 < \Psi \leq 1$, which proves crucial in view of the potential stagnation points ($Q = 0$) on $\Psi = 0$ far upstream ($\Phi = -\infty$) and at $\Phi = 0$.

From integrating (46) Bernoulli's law giving the first integral of motion $B(\Psi)$ ensues:

$$Q^2/2 + P = B(\Psi), \quad B' = -\Omega \quad (50)$$

is confirmed by (47) with (48). One infers from (44) that the curvature of streamline reads $\chi Q\Theta_\Phi$, thus the Laplace pressures $\tau(Q\Theta_\Phi)(\Phi, 1)$ and $-\tau(\chi Q\Theta_\Phi)(\Phi, 0)$. Hence, (12) combined with (14) result into mixed BCs,

$$\Psi = 1: \quad \tau Q\Theta_\Phi = B(1) - \frac{Q^2}{2}, \quad \Psi = 0: \quad \chi Q\Theta_\Phi = \begin{cases} \theta'_w(s) & (\Phi \leq 0), \\ [Q^2/2 - B(0)]/\tau & (\Phi > 0). \end{cases} \quad (51)$$

Evaluating the condition for $\Psi = 0$ upstream of detachment invokes the dependence of the arc length s along the wall and Φ . This is readily inferred from (44) as $d\Phi/ds|_{\Psi=0} = (\chi Q)(\Phi, 0)$, entailing the auxiliary relationship

$$s - s_D = \int_0^\Phi \frac{dt}{(\chi Q)(t, 0)}. \quad (52)$$

Typically, the position of detachment $s = s_D$ can be chosen arbitrarily in an inviscid-flow calculation. It is therefore distinguished from the actual one, $s = s_d$, found for finite values ϵ . However, we will see how to determine $s_d \sim s_D$ in advance as $\epsilon \rightarrow 0$.

Finally, the far-upstream and -downstream BCs are stated using (50) as

$$\Phi \rightarrow \pm\infty: \quad Q \rightarrow Q_\infty(\Psi) = \sqrt{2B(\Psi)}, \quad \Phi \rightarrow -\infty: \quad \Theta \rightarrow 0. \quad (53)$$

Prescribing $Q_\infty = \psi'_-(n)$, see § 3.4.1, using the inversion $n = \psi^{-1}(\Psi)$ fixes $B(\Psi)$. From (49) then follows the missing far-field condition $\chi(\pm\infty, \Psi) = Q_\infty(1)/Q_\infty(\Psi)$. The discussion of the BCs for $s \rightarrow \pm\infty$ closing § 3.2 remains valid here to some extent. Most importantly, here the requirement of vanishing streamline curvature far downstream in connection with (48) forces the inviscid flow to fully recover and attain its oncoming state. The uniform turning angle, $\Theta_+ = \Theta(+\infty, \Psi)$, is also part of the solution of the well-posed elliptic Euler problem we have established. Consisting of (45), (48), (49) and (51)–(53), it governs Q and Θ once the position $s = s_d$ of detachment has been chosen adequately.

5.2 Solution strategy and solution properties

The solution depends strongly on the properties of $B(\Psi)$, where two most essential ones account crucially for the pressure-free incident flow, hence implying $B(\Psi) = Q_\infty^2/2$. At first, the free slip on the upper free streamline gives $B'(1) = \Omega(1) = 0$. Secondly, with the constant σ denoting the terminal wall shear stress of the oncoming layer, one reveals $\psi_-(n) = \sigma n^2/2 + O(n^5)$ ($n \rightarrow 0$) and, in turn, $B(\Psi) = \sigma\Psi + O(\Psi^{5/2})$ ($\Psi \rightarrow 0$). Due to this initial stagnation on the wall, the flow first accelerates as the pressure decreases according to (50). We will elucidate how this behaviour has a crucial impact on detachment.

One then advantageously eliminates Θ from (45), (48) and (51) using (49) to obtain

$$(\chi Q_\Phi/Q)_\Phi + [\chi^{-1}(\chi Q)_\Psi/(\chi Q)]_\Psi = 0, \quad (54)$$

$$\Psi = 1: \tau Q_\Psi = \frac{Q^2}{2} - B(1), \quad \Psi = 0: \frac{\sigma}{Q} - Q_\Psi = \begin{cases} \theta'_w(s) & (\Phi \leq 0), \\ [Q^2/2 - B(0)]/\tau & (\Phi > 0). \end{cases} \quad (55)$$

These relationships complemented with by (49), (52) and (53) pose a problem governing Q on the stripe $-\infty < \phi < \infty$, $0 \leq \psi \leq 1$, parametrised by τ , s_d and $B(\psi)$. The flow angle Θ and the locations of the streamlines in the physical plane can be readily found a posteriori from integrating (48) on $\Psi = \text{const}$. The aforementioned inversion at $\Phi = -\infty$ yields the initial elevation of the streamlines above the wall. Although numerically demanding and highly nonlinear, this inviscid-flow problem is yet much easier to tackle than the full NS problem for realistically small values of ϵ . As it stands, it is ripe for its numerical solution with finite differences and/or Chebychev collocation, advantageously after mapping the stripe onto the unit square once the asymptotic corrections to the limits in (53) have been determined.

Of utmost interest is the detachment or *apparent* contact angle Θ_D , in sharp contrast with the actual one, θ_c , here following from the computed flow angle $\Theta(0+, 0)$ immediately downstream of detachment, cf. (13):

$$\theta_w(s_D) - \Theta(0+, 0) = \pi - \Theta_D. \quad (56)$$

One can identify Θ_D with θ_c (and thus prescribe s_D) only in the hypothetical case of a perfectly ideal fluid ($\tilde{\nu} = \epsilon = 0$), apart from the exceptional situation of a fluid entirely at rest (as a sessile droplet). In any other case, θ_D is part of the inviscid-flow solution. Due to the lack of any further physical length scale, the detachment angle θ_D indeed cannot be altered if one introduces some artificial smaller scale to describe the potential flow around the detachment point: in general, $\theta_D < \pi$, and a stagnant wedge flow describes detachment locally. However, we anticipate at this stage that tangential detachment,

$$\Theta_D = \pi, \quad (57)$$

is the rule rather than the exception as (57) sorts out the only acceptable situation that is not in conflict with BL separation in the limit $\epsilon \rightarrow 0$. This result holds for $\tau \geq 0$, but the limit $\tau \rightarrow 0$ applied to the above Euler problem is also singular.

In the present context, the relevance of the TC speed can also be inferred from the cross-stream momentum balance (47) supplemented with (51) in case of a free jet ($\Phi > 0$). It is first observed that (45) and (48) allow for a parallel-flow solution $Q = Q(\Psi)$, hence $\chi = Q(1)/Q(\Psi)$ by (49), and $\Theta = \Theta(\Phi)$ where $\Theta' = K = \text{const}$ is the (non-zero) curvature of the then parallel streamlines. This situation might also apply to the leading-order description of a slender layer in the long-wave limit. Now on integration of (47)

using the notation in (18) and $P(1) = \tau Q(1)K$, $P(0) = -\tau Q(1)K$, see (51),

$$Q(1)KJ = P(1) - P(0) = 2\tau Q(1)K \quad \text{or} \quad T = 1/2. \quad (58)$$

That is, such a flow can only exist if T is locked to $1/2$ and thus assumes the TC speed if it is irrotational. The linkage to the long sinusoidal Taylor–Squire modes of small amplitude (§3.4.2) is striking.

To the author’s knowledge, the only solution of an inviscid free-surface flow problem of the type negotiated here, i.e. with vorticity fully at play and no ad-hoc slenderness assumption made, presently available must be attributed to Pasias (2022). In this work, a closely related situation is considered, but no curved wall.

5.3 Potential flow

Drastic simplifications arise if one assumes *ad-hoc* an irrotational flow, hence $\chi \equiv 1$, preferably normalised by $Q_\infty \equiv 1$. Although a potential flow does not match the (realistic premise of a) developed flow far upstream, elegantly exploiting the well-established semi-analytical conformal-mapping techniques allows for gaining a profound understanding of how inertia controls the teapot effect. The hydrodynamic retention force can be predicted in straightforward manner. Most rational studies of the teapot effect rely on the potential-flow assumption, but so far at the expense of the entire neglect of capillarity and thus reducing the underlying physics to inertia and partially gravity.

5.3.1 Outline

The first as early as by Keller (1957) predicted analytically the complete turn of $\theta_+ = \pi$ for a flow around a thin plate, i.e. having sharp trailing edge and thus a concentrated retention force. He also considered the gravitational influence. The first of the refinement by Vanden-Broeck & Keller (1986, 1989) took into account a wedge-shaped lip and gravity from the start, which requires a numerical treatment. The second ignored gravity again and thereby put forward an analytic solution for the flow found to detach from the underside of the wedge. As a further advancement, it also deals with its concavely shaped underside, where the solution had to be constructed numerically. The inclusion of surface tension has been only addressed in Chapman & Vanden-Broeck (2002), albeit under the assumption of strictly attached flow, i.e. having just one free surface.

The numerical method at play in these studies is the so-called series truncation method. Here the complex flow potential $w = \Phi + i\Psi$ and velocity potential $\zeta(w) = Q \exp(i\Theta)$ are mapped consecutively conformally in an advantageous, problem-specific manner, finally onto the half of a unit circle in an auxiliary complex plane. In its interior, ζ is found via collocation on its boundaries which represent the free streamlines and solid walls in the problem. The flow is then reconstructed in the physical plane by calculating the potential $z(w) = x + iy$ where x, y denote appropriately positioned Cartesian coordinates. It is often useful to also consider $\varpi(W) = \ln \zeta = V + i\Theta$, $V = \ln Q$. For expanding upon this technique see (Vanden-Broeck, 2010, chap. 6.2), e.g. its recent application to long-standing hydraulic problems by McLean et al. (2022). We also refer to a related method suggested by Eggers & Smith (2010).

To study the flow near detachment, one advantageously rewrites (50) as $Q^2/2 - \tau Q \Theta_\Phi = 1/2$ for $\Phi > 0$ or

$$\Psi = 0, \quad \Phi > 0: \quad \sinh V = \tau \Theta_\Phi, \quad V = \text{Re } \varpi, \quad \Theta = \text{Im } \varpi. \quad (59)$$

Without any substantial loss of generality, we hereafter ignore the local slope of the wall by identifying Θ with $\Theta - \theta_w(s_D)$. As consistent with our previous notation, Θ then is the flow angle measured relative to the wall in the clockwise direction such that $\Theta_D < 0$. Since this is taken as sufficiently smooth, it is locally replaced by a straight line. Then for

$$\Psi = 0, \quad \Phi \leq 0: \quad \Theta = 0. \quad (60)$$

This kinematic BC complements the dynamic one (59) to mixed BCs, determining ζ or ϖ in terms of local eigensolutions in the limit $w \rightarrow 0$. The most essential findings are summarised in the following. An important ingredient here is the potential loss of analyticity of ϖ in $w = 0$ as it can in general behave logarithmic–algebraically locally. We refer to the [Vanden-Broeck \(2010\)](#), in particular chaps. 3.1.2 and 3.2.2 therein surveying irrotational separation from a smooth surface in great detail.

5.3.2 Neglect of surface tension

If $\tau = 0$, (59) predicts the recovery $Q = 1$, $V = 0$ at and downstream of then tangential detachment ($\theta_D = 0$). It is easily seen that the general behaviour is

$$\varpi = i\beta(s_D) w^{1/2} + O(w^{3/2}), \quad \beta \geq 0 \quad (w \rightarrow 0). \quad (61)$$

The dominant term in this expansion indicates the famous Brillouin–Villat (BV) singularity, characteristic of purely inertia-driven irrotational free-streamline separation and having some strength β that depends on the, yet largely arbitrary, position of its occurrence. For $\beta \neq 0$, $\Theta(Q)$ behaves regular (singular) as $s \rightarrow s_D^-$ but irregular (regular) as $s \rightarrow s_D^+$. In particular, the streamline detaches with infinite curvature as $\Theta(Q)$ are here constant upstream (downstream) of detachment. The degenerate case $\beta = 0$ is commonly referred to as BV condition, a notion becoming evident in § 6. For positive values of β , (50) predicts an pressure increase as the flow just approaches detachment, negative ones are prohibited on geometrical grounds (the free streamline would immediately intersect the wall).

5.3.3 Influence of surface tension

Here we give only the general result that describes the flow around a concave wedge where the free surface forms the downstream portion of its boundary. It is illuminating to express it for $z(w)$ where x, y have heir origin in the detachment point, x points tangentially to the wall upstream of detachment in the flow direction and y normally to it. Successive evaluation of (59) and (60) and the requirement that $\Psi = 0$ determines the position z of the free streamline then reveal a Taylor expansion in terms of the dominant formulation of a wedge-flow (only this seems to be treated in the existing literature):

$$z = \sum_{k=1}^{\infty} \beta_k(s_D, \tau) e^{-ik\Theta_D} w^{k(1+\Theta_D/\pi)}, \quad \beta_k \in \mathbb{R}, \quad (w \rightarrow 0). \quad (62)$$

Only the dominant coefficient β_1 is fixed by the global flow; for any $k > 1$, β_k then follows from (59). Specifically,

$$\beta_2 = -\beta_1^2 / (4\tau \sin \Theta_D) (> 0). \quad (63)$$

The expansion (62) also predicts an retarded flow upstream of but stagnation at detachment. Investigating the limit $\Theta \rightarrow 0^-$ discloses the exceptional situation of tangential detachment at some $s_D = s_D^*(\tau)$, where the pressure increase immediately ahead

of detachment vanishes. Evidently, a similar situation is found if we let $\tau \rightarrow 0$. As an important consequence, s_D^* must approach the value at which the BV condition is fulfilled in the limit $\tau \rightarrow 0$. Problems subjected to this type of limit process fall under the category of selection problems. The current example illustrates the fundamental mechanism: the flow for finite values of τ “selects” the correct member out of a one-parametric family of flows having $\tau = 0$ from the outset and thus controlled solely by s_D (see [Vanden-Broeck, 2010](#), chap. 3.2).

6 Regularising Role of Viscosity and Selection Problems

Finally, we briefly address the two central modifications of the inviscid flow in the singular limit $\epsilon \rightarrow 0$. Most importantly, the first renders it unique as it fixes the position $s = s_D$ of break-away. The second concerns the transition of the terminal state of the parallel Euler flow having finite vorticity towards the fully homogenous one for $s \rightarrow \infty$ over a long streamwise scale of $O(\epsilon)$.

6.1 Position of and structure around detachment

The adverse pressure gradient the inviscid flow exerts on the wall as it approaches detachment becomes infinite there while the BV singularity, if $\tau = 0$, has a finite strength $\beta > 0$ or, if $\tau > 0$, detachment is wedge-type. In both cases, it is a well-established fact that the BL would terminate further upstream (in terms of the well-known Goldstein singularity) as it cannot withstand such an unbounded pressure gradient. Therefore, a self-consistent (asymptotically correct) flow description in the limit $\epsilon \rightarrow 0$ requires β to vanish if $\tau = 0$ but also pure tangential detachment if $\tau > 0$, as claimed by (57). In other words, in both cases the position of detachment of the inviscid flow must be chosen such that $P_\Phi(0, \Psi) < 0$ upstream of $s = s_D$ and $P_\Phi(0, \Psi) = 0$ for $s = s_D$. Calculations for finite values of ϵ will show this variation of the detachment point once ϵ becomes arbitrarily small. Therefore, this type of regularisation must also be categorised as a selection process: now the viscous flow “selects” the correct member in class of potential flows parametrised by s_D to accommodate to it.

For single-phase stationary gross separation ($\tau = 0$), this adaption is well understood and accomplished by triple-deck theory. This accounts for the correct splitting of the BL due to the shortening of the streamwise scale and the local breakdown of the classical hierarchical scheme of matched asymptotic expansion governing the oncoming BL, in favour of a strong localised interaction between the self-induced pressure gradient, suitably smoothing the imposed one, and the associated displacement exerted by the viscous near-wall portion of the just detaching BL. Finally, this mechanism effectively regularises a BV singularity of a strength $\beta = O(\epsilon^{1/16})$. For the details the reader is referred to the survey by [Sychev et al. \(1998, chap. 1\)](#) and the original solution to the triple-deck problem by [Smith \(1977\)](#) (and the references therein). In the situation of §4, the – yet unavailable – counterpart of this flow description including surface tension would give the correct answer to the embedding of the Stokes flow observed on the smallest scale, where it negotiates the real, chemical contact angle $\theta_c < \pi$, into the BL. Considering an appropriate distinguished limit $\tau \rightarrow 0$ as $\epsilon \rightarrow 0$, hence starting with a vanishingly weak BV singularity at inviscid flow detachment, presumably provides the first sensible step towards unravelling this demanding question of perturbation theory.

As demonstrated by [Vanden-Broeck & Keller \(1989\)](#), the BV condition can only be met if the underside of the wedge-shaped lip is (concavely) curved. Therefore, if straight

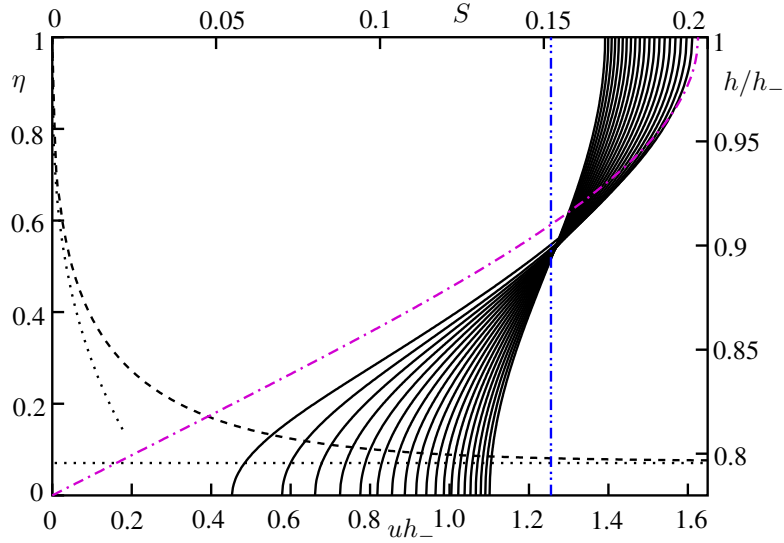


Figure 6: Evolution of detached shear layer flow for $S = 0.005i$, $i = 0, 1, \dots, 20$ (left to right): scaled flow profiles $u h_-$, from Watson's self-preserving ($S = 0$, dash-dotted) to uniform flow ($S = 0.999$, dash-dot-dotted), and vertical height (dashed, top abscissa) with leading-order asymptotes (dotted) found for $S \rightarrow 0$ (Goldstein wake) and $S \rightarrow \infty$ ($h = h_+$).

lines form its walls, only the trivial solution of a uniform parallel flow passing its sharp tip as undisturbed is the acceptable selection for $\epsilon = 0$.

6.2 Terminal evolution of free jet

Given the recovery of a stagnant flow on $\Psi = 0$, ensuing from the properties of $B(\Psi)$ addressed in § 5.2 and § 3.4.1, we notice a viscous shear layer astride the lowermost streamline smoothing the shear rate σ at the base of the Euler flow. This produces a slip (increasing from zero) along the lower free surface. Far downstream, the flow in this viscous sublayer assumes the self-similar form of the well-known Goldstein wake (GW). Since its width becomes of $O(\epsilon s)^{1/3}$, it merges with the whole jet and triggers a redistribution of vorticity over the long scale where $S = s/(\epsilon h_-) = O(1)$. There (9) reduces to shallow-water form and describes a pressure-free shear layer bounded by two free streamlines to leading order. Capillarity has become a higher-order effect. The evolution of the flow over S towards the uniform one ($u = u_+$, $h = h_+$) provides the slowly varying background flow in the WKBJ analysis brought up in § 3.3.

We present its development by numerical marching, where the incident recovered flow is given by Watson's self-similar one (§ 3.4.1), in figure 6: the results are extracted from Scheichl, Bowles & Piasias (2018) as the developed flow passing a sharp trailing edge raises the same problem over that viscous length scale. Its terminal modification on that scale is initiated by the GW, there forming immediately downstream of the plate edge ($S = 0$). Hence, $h/h_- = 1 + O(S^{1/3})$ as $S \rightarrow 0$. Accordingly, the requirement that the GW exerts zero vertical displacement of the streamlines in leading order yields a cuspidal shape of the just forming lower free streamline. Otherwise, its vertical transfer would provoke an associated singularity in the upper free streamline and an accordingly large streamline curvature. This would produce an unacceptably large streamwise pressure gradient due to the cross-stream momentum transfer.

7 Final remarks

This synopsis presents selected ingredients to the holistic asymptotic analysis of the teapot effect and related free-surface flows where inertia effects are dominantly at play at the outset. It points to the foci of the ongoing activities in this thrust of research. Further aspects and specific technical details will be put forward during the lectures and in the book chapter. In particular, the integral conservation of linear momentum will also be envisaged. This final form of these lecture notes will also be disseminated to the participants of the course.

References

- BOUWHUIS, W. & SNOELJER, C.H. 2015 The effect of surface wettability on inertial pouring flows. DOI: [10.48550/arXiv:1507.05931](https://doi.org/10.48550/arXiv:1507.05931).
- CHAPMAN, S.J. & VANDEN-BROECK, J.-M. 2002 Exponential asymptotics and capillary waves. *SIAM J. Appl. Math.* **62** (6), 1872–1898. DOI: [jstor.org/stable/3648744](https://doi.org/jstor.org/stable/3648744).
- CULICK, F.S.C. 1960 Comments on a ruptured soap film. *J. Appl. Phys.* **31** (6), 1128–1129. DOI: [10.1063/1.1735765](https://doi.org/10.1063/1.1735765).
- DUEZ, C., YBERT, CH., CLANET, CH. & BOCQUET, L. 2010 Wetting controls separation of inertial flows from solid surfaces. *Phys. Rev. Lett.* **104** (8), 084503-1–084504-4. DOI: [10.1103/PhysRevLett.104.084503](https://doi.org/10.1103/PhysRevLett.104.084503).
- DRAZIN, P.G. & REID, W.H. 2004 *Hydrodynamic Stability*, 2nd ed., Cambridge Mathematical Library. Cambridge University Press.
- DYSON, D.C. 1988 Contact line stability at edges: Comments on Gibbs’s inequalities. *Phys. Fluids* **31** (2), 229–232. DOI: [10.1063/1.866851](https://doi.org/10.1063/1.866851).
- EGGERS, J. & SMITH, A. F. 2010 Free streamline flows with singularities. *J. Fluid Mech.* **647**, 187–200. DOI: [10.1017/S0022112009993624](https://doi.org/10.1017/S0022112009993624).
- FRAENKEL, L.E. & SQUIRE, H.B. 1962 Laminar flow in symmetrical channels with slightly curved walls, I. On the Jeffery–Hamel solutions for flow between plane walls. *Proc. R. Soc. Lond. A* **267** (1328), 119–138. DOI: [10.1098/rspa.1962.0087](https://doi.org/10.1098/rspa.1962.0087).
- GAJJAR, J.S.B. 1987 Fully developed free surface flows—Liquid layer flow over a convex corner. *Comput. Fluids* **15** (4), 337–360. DOI: [10.1016/0045-7930\(87\)90028-4](https://doi.org/10.1016/0045-7930(87)90028-4).
- GUYON, E., HULIN, J.P., PETIT, L., MITESCU, C.D. 2001 *Physical Hydrodynamics*, 2nd ed. Oxford University Press. DOI: [10.1093/acprof:oso/9780198702443.001.0001](https://doi.org/10.1093/acprof:oso/9780198702443.001.0001).
- HIGUERA, F.J. 1994 The hydraulic jump in a viscous laminar flow. *J. Fluid Mech.* **274**, 69–92. DOI: [10.1017/S0022112094002041](https://doi.org/10.1017/S0022112094002041).
- KELLER, J. B. 1957 Teapot effect. *J. Appl. Phys.* **28** (8), 859–864. DOI: [10.1063/1.1722875](https://doi.org/10.1063/1.1722875).
- KISTLER, S.F. & SCRIVEN, L.E. 1994 The teapot effect: sheet-forming flows with deflection, wetting and hysteresis. *J. Fluid Mech.* **263**, 19–62. DOI: [10.1017/S0022112094004027](https://doi.org/10.1017/S0022112094004027).

- MCLEAN, E., BOWLES R., SCHEICHL, B. & VANDEN-BROECK, J.-M. 2022 Improved calculations of waterfalls and weir flows. *J. Fluid Mech.* **941** (A27). DOI: [10.1017/jfm.2022.305](https://doi.org/10.1017/jfm.2022.305).
- MOFFATT, H.K. 1964 Viscous and resistive eddies near a sharp corner. *J. Fluid Mech.* **18** (1), 1–18. DOI: [10.1017/S0022112064000015](https://doi.org/10.1017/S0022112064000015).
- PASIAS, G. 2022 Developed liquid film passing a trailing edge under the action of gravity and capillarity. PhD thesis, Dept. of Mathematics, University College London. Open access at UCL Discovery: discovery.ucl.ac.uk/id/eprint/10152957/.
- REINER, M. 1956 The teapot effect... a problem. *Phys. Today* **9** (9), 16–20. DOI: [10.1063/1.3060089](https://doi.org/10.1063/1.3060089).
- SCHEICHL, B., BOWLES, R.I. & PASIAS, G. 2018 Developed liquid film passing a trailing edge under the action of gravity and capillarity. *J. Fluid Mech.* **850**, 924–953. DOI: [10.1017/jfm.2018.464](https://doi.org/10.1017/jfm.2018.464).
- SCHEICHL, B., BOWLES, R.I. & PASIAS, G. 2021 Developed liquid film passing a smoothed and wedge-shaped trailing edge: small-scale analysis and the ‘teapot effect’ at large Reynolds numbers. *J. Fluid Mech.* **926** (A24). DOI: [10.1017/jfm.2021.612](https://doi.org/10.1017/jfm.2021.612).
- SMITH, F.T. 1977 The laminar separation of an incompressible fluid streaming past a smooth surface. *Proc. R. Soc. Lond. A* **356** (1687), 443–463. DOI: [10.1098/rspa.1977.0144](https://doi.org/10.1098/rspa.1977.0144).
- SQUIRE, H.B. 1953 Investigation of the instability of a moving liquid film. *Brit. J. Appl. Phys.* **4** (86), 167–169. DOI: [10.1088/0508-3443/4/6/302](https://doi.org/10.1088/0508-3443/4/6/302).
- SYCHEV, V.V., RUBAN, A.I., SYCHEV VIC.V. & KOROLEV, G.L. 1998 *Asymptotic theory of separated flows*. Cambridge University Press. DOI: [10.1017/CBO9780511983764](https://doi.org/10.1017/CBO9780511983764).
- TANEDA, S. 1979 Visualization of separating Stokes flows. *J. Phys. Soc. Jpn.* **46** (6), 1935–1942. DOI: [10.1143/JPSJ.46.1935](https://doi.org/10.1143/JPSJ.46.1935).
- TAYLOR, G.I. 1959a The dynamics of thin sheets of fluid. II. Waves on fluid sheets. *Proc. R. Soc. Lond. A* **253** (1274), 296–312. DOI: [10.1098/rspa.1959.0195](https://doi.org/10.1098/rspa.1959.0195).
- TAYLOR, G.I. 1959b The dynamics of thin sheets of fluid. III. Disintegration of fluid sheets. *Proc. R. Soc. Lond. A* **253** (1274), 313–321. DOI: [10.1098/rspa.1959.0196](https://doi.org/10.1098/rspa.1959.0196).
- TU WIEN 2021 Why teapots always drip. *TU Wien News*, 08. November 2021.
- VANDEN-BROECK, J.-M. 2010 *Gravity–Capillary Free-Surface Flows*, Cambridge Monographs on Mechanics. Cambridge University Press. DOI: [10.1017/CBO9780511730276](https://doi.org/10.1017/CBO9780511730276).
- VANDEN-BROECK, J.-M. & KELLER, J.B. 1986 Pouring flows. *Phys. Fluids* **29** (12), 3958–3961. DOI: [10.1063/1.865735](https://doi.org/10.1063/1.865735).
- VANDEN-BROECK, J.-M. & KELLER, J.B. 1989 Pouring flows with separation. *Phys. Fluids A* **1** (1), 156–158. DOI: [10.1063/1.857542](https://doi.org/10.1063/1.857542).
- VAN DYKE, M.D. 1975 *Perturbation Methods in Fluid Mechanics*, Annotated edition. Parabolic Press.

WALKER, J. 1984 The troublesome teapot effect, or why a poured liquid clings to the container (“The Amateur Scientist”). *Sci. Am.* **251** (4), 144–153. DOI: [jstor.org/stable/e24969444](https://doi.org/10.1017/S0022112064001367).

WATSON, E.J. 1964 The radial spread of a liquid jet over a horizontal plane. *J. Fluid Mech.* **20** (3), 481–499. DOI: [10.1017/S0022112064001367](https://doi.org/10.1017/S0022112064001367)